Marine Chemistry 224 (2020) 103808

Contents lists available at ScienceDirect

Marine Chemistry

journal homepage: www.elsevier.com/locate/marchem

Trace element and Sr isotopic composition of bottom and near-surface oceanic water in the southern region of the Emperor Ridge

I.A. Vishnevskaya[a,b,c,*], T.G. Okuneva[b], D.V. Kiseleva[b], N.G. Soloshenko[b], M.V. Streletskaya[b], Yu.S. Vosel[d]

[a] Vernadsky Institute of Geochemistry and Analytical Chemistry, RAS, 119334 Moscow, 19 Kosygina str., Russia
[b] Zavaritsky Institute of Geology and Geochemistry, UB RAS, 620016 Ekaterinburg, 15 Akademika Vonsovskogo str., Russia
[c] Novosibirsk State University, 630090 Novosibirsk, 2 Pirogova str., Russia
[d] Institute of Geology and Mineralogy named after V.S. Sobolev, SB RAS, 630090 Novosibirsk, 3 Akademika Koptyuga ave., Russia

ARTICLE INFO

Keywords:
$^{87}Sr/^{86}Sr$ ratio
Vertical mixing
Ocean water composition
North Pacific Ocean
Hawaiian Emperor bend
Emperor chain

ABSTRACT

During the 86th voyage of the research vessel "Akademik M.A. Lavrentiev" (July–August 2019), near-bottom and near-surface water samples (at a depth of 10 m) were taken in the immediate vicinity and above the Koko, Jingu, Nintoku, and Suiko seamounts in the southern part of the Emperor seamount chain. Trace element concentrations (including REE) in these samples are higher than in the IAPSO Standard Atlantic Seawater. The distribution and mutual correlations of elements involved in biochemical processes indicate an active role of plankton in the accumulation of these elements, as well as an increase in its amount with increasing water temperature. $^{87}Sr/^{86}Sr$ ratios in water samples vary from 0.70891 to 0.70917. Moreover, near-bottom water, taken farther south of 44°N, is more radiogenic than near-surface. This difference can be explained by the dilution of the surface layer with meteoric water, because at the time of sample collection over the Koko, Jingu, and Nintoku seamounts it was raining daily, while no rainfall was observed over the Suiko seamount during the sample collection and the week before it. The rapid restoration of isotopic equilibrium indicates a high rate of vertical mixing of ocean water, which was indicated by the earlier studies of oceanic water chemical composition.

1. Introduction

Sr isotopic composition of ocean water is formed due to the mixing of several Sr sources with different isotopic characteristics. The destruction material of continental rocks with a high $^{87}Sr/^{86}Sr$ ratio is brought into the ocean basin by rivers, glaciers and wind (currently the isotopic composition of the continental runoff is estimated at 0.7116 (Davis et al., 2003)). At the same time, during the destruction of mid-ocean ridge basalts, as well as the halmirolysis of ocean floor rocks, Sr with a low $^{87}Sr/^{86}Sr$ ratio enters the water (now it is 0.7037 (Bach and Humphris, 1999)). Slightly less powerful sources of Sr are sea carbonates, which release upon recrystallization a part of the average isotopic composition of Sr held in the crystal lattice, which is 0.7084 (Elderfield and Gieskes, 1982). Due to the fact that Sr residence time in seawater is three orders of magnitude higher than the time of complete mixing of ocean waters (Broecker and Peng, 1982; Elderfield and Greaves, 1982), Sr isotopic composition manages to be completely averaged until it is fixed in the sediment. At present, $^{87}Sr/^{86}Sr$ ratio in the oceans is 0.70917 (Burke et al., 1982; Faure, 1986; Hodell et al., 1989; Banner, 2004; McArthur et al., 2001, 2012; Kuznetsov et al., 2014, 2018, and references in these works).

Change in the balance between continental and mantle flows is reflected in the Sr isotopic composition of the world ocean and therefore $^{87}Sr/^{86}Sr$ ratio varies over time (geological history). Such a change is reflected in the global variation curve of $^{87}Sr/^{86}Sr$ ratio (DePaolo, 1987; McArthur et al., 2001, 2012; Halverson et al., 2007, 2010; Sawaki et al., 2010; Kuznetsov et al., 2014, 2018), which has minima comparable to global periods of extension and plume activity. The maxima, in turn, reflect the periods of high standing of the continents, during which an increase in erosion and the proportion of crustal material in the sedimentation basins occurs. This variation curve is widely used in determining the age of sedimentary chemogenic rocks.

The process of ocean water mixing, which provides the uniformity of Sr isotopic composition, is very complex and consists of both horizontal and vertical currents. Horizontal mixing is believed to be more effective than vertical mixing (Gregg, 1991). However, near oceanic boundaries, such as surface mountains and mid-ocean ridges, the contribution of the vertical component increases (Stewart, 2008; Darnitsky,

* Corresponding author at: Vernadsky Institute of Geochemistry and Analytical Chemistry, RAS, 119334 Moscow, 19 Kosygina str., Russia.
E-mail address: vishnevskaia@geokhi.ru (I.A. Vishnevskaya).

https://doi.org/10.1016/j.marchem.2020.103808
Received 6 January 2020; Received in revised form 14 April 2020; Accepted 14 April 2020
Available online 18 April 2020

2010). The distribution of chemical elements does not depend on stratification by salinity, and the temperature of ocean water and is controlled only by the rate of molecular mixing (England and Maier-Reimer, 2001; Jenkins, 2004).

Sr isotopic composition of ocean and sea water is often studied by measuring the $^{87}Sr/^{86}Sr$ ratio in bottom sediment columns or in mollusk shells taken on sea shores (Banner, 2004; McArthur et al., 2012; Kuznetsov et al., 2014, 2018, and references in these works), while the detailed studies of Sr and trace element behavior in the ocean water are rather scarce. The present study is aimed to indicate spatial variations in the chemical and Sr isotopic composition of ocean water at the surface and at a depth of 1–2 km in order to trace the mixing processes of water masses.

2. Materials and methods

2.1. Sampling location and water samples

86th voyage of the research vessel "Akademik M.A. Lavrentiev" was held in July–August 2019. The aim of the expedition was a comprehensive study of the seamounts of the southern part of the Emperor seamount chain. The ridge includes more than a dozen seamounts - extinct volcanoes. The northernmost Meiji volcano is considered to be the oldest, its age is estimated as 85 Ma (Keller et al., 2000). The youngest - Daikakuji – is 42 million years (Dalrymple and Clague, 1976), it is articulated to the Hawaiian ridge. The volcanic structures of the southern part of the ridge are composed of tholeiitic and alkaline basalts (Clague and Dalrymple, 1987).

The region belongs to the subtropical climate zone. Storms are rare throughout the year. According to https://earth.nullschool.net/, the coldest and driest period lasts from late December to early April, with average temperatures ranging from 13 to 17 °C. The warmest and at the same time humid time falls on July–September, the average temperature during this period is around 25 °C.

The Carousel Water Sampler system was used for water sampling at predetermined horizons at depths of up to 6000 m, equipped with 12 5-l Niskin bathometers and a set of research equipment: SBE 19 plus temperature, depth, and salinity sensors, as well as SBE 43 dissolved oxygen sensor.

Water samples for trace element and Sr isotopic analyses were taken directly from the Niskin bathometer into 15 ml Axygen® polyethylene tubes with screw caps. The samples were stored unfiltered and unacidified, with Parafilm® wrapped around the cap. The possibility of storing water samples without filtering and acidifying was shown earlier by the repeated analyses of selected oceanic water samples, which indicated no measurable signs of evaporation after one year of storage, as well as no measurable difference between filtered/unfiltered or acidified/unacidified samples (de Villiers, 1999).

12 samples were taken: two samples in the area of the Koko and Jingu seamounts, 4 in the areas of Nintoku and Suiko seamounts (Fig. 1). They were taken from the near-surface horizon at a depth of 10 m and from the bottom layer. The bottom layer at different points was at different depths (Table 1), but always in 50 m from the bottom. Due to technical reasons, sample collecting from interim depths as well as rainwater was not implemented.

2.2. Reagents and certified reference materials

All sample preparation procedures were performed in cleanrooms (class 1000) and laminar boxes (class 100) of the Zavaritsky Institute of Geology and Geochemistry, Ekaterinburg, Russia. HCl and HNO_3 ACS grade acids were additionally purified twice using sub-boiling purification systems (Savillex, USA; Berghof, Germany). Deionized water (18.2 $M\Omega cm^{-1}$) was obtained by Arium®pro unit (Sartorius, Germany). All the labware and materials contacting the reagents and samples were made of PFA (Savillex, USA) or PTFE (Nalgene, USA). Polypropylene columns (Triskem®, France) fitted with two 35 μm PE frits were used. Prior the analysis, extra cleaning was performed to columns, pipette tips and PFA vials (Savillex®). Pipette tips and columns were washed with $HCl:H_2O$ (1:1) on a hotplate overnight and then rinsed with deionized water. The vials were pre-cleaned by boiling in 1:3 mixture of HNO_3 and HCl overnight with subsequent boiling in deionized water. NIST SRM-987 certified reference material was applied to control the isotopic measurement procedure.

2.3. Trace element ICP-MS measurements

Isotope measurements were conducted in cleanrooms (class 10,000) of the Zavaritsky Institute of Geology and Geochemistry, Ekaterinburg, Russia. A 5 ml portion of each sample was quantitatively transferred into polypropylene containers, then added 100 μl of In (internal standard) solution (1 mg/l) and 150 μl of 14 M HNO_3 and diluted to a volume of 10 ml with ultrapure water in order to keep the final HNO_3 concentration at 3% (v/v).

Calibration curves were constructed using multi-element standard solutions (Inorganic Ventures).

A NexION 300S (PerkinElmer, USA) quadrupole mass-spectrometer was used for the quantitative determination of the following isotopes: ^{7}Li, ^{9}Be, ^{45}Sc, ^{47}Ti, ^{51}V, ^{53}Cr, ^{55}Mn, ^{59}Co, ^{60}Ni, ^{65}Cu, ^{66}Zn, ^{71}Ga, ^{74}Ge, ^{75}As, ^{82}Se, ^{85}Rb, ^{86}Sr, ^{89}Y, ^{90}Zr, ^{93}Nb, ^{95}Mo, ^{109}Ag, ^{111}Cd, ^{118}Sn, ^{123}Sb, ^{128}Te, ^{133}Cs, ^{135}Ba, ^{139}La, ^{140}Ce, ^{141}Pr, ^{146}Nd, ^{147}Sm, ^{153}Eu, ^{157}Gd, ^{159}Tb, ^{163}Dy, ^{165}Ho, ^{167}Er, ^{169}Tm, ^{172}Yb, ^{175}Lu, ^{178}Hf, ^{181}Ta, ^{184}W, ^{205}Tl, ^{208}Pb, ^{209}Bi, ^{232}Th, ^{238}U.

NexION 300S instrumental parameters for the ICP-MS solution analysis were as follows: RF power 1300 W, plasma gas flow rate 16 l/min, auxiliary gas flow rate 1.0 l/min and sample gas flow rate (Ar) 1 l/min. The control of the correctness and accuracy of determining the trace element composition was carried out using certified multi-element solutions (Inorganic Ventures). The obtained concentrations of trace elements are in satisfactory agreement with certified values with an allowable deviation within 15%. Duplicate analyses of seawater samples typically yielded an error less than 5%.

2.4. Sample concentration and ion exchange chromatography

The amount of water sample, containing ca. 600 ng of Sr, was placed in a PFA vial and evaporated to dryness on a hotplate at 120 °C. Then, the residue was dissolved in 0.5 ml of 7 M HNO_3, placed in an Eppendorf microtube and centrifuged at 6000 rpm for 15 min by EBA 21 centrifuge (Hettich, Germany). Single-step chromatography technique modified from (Muynck et al., 2009) and described in (Kasyanova et al., 2019) was applied for strontium isolation. SR resin (100–200 mesh, Triskem®) was loaded into pre-cleaned columns with the following layer configuration: D = 0.7 cm, h = 3 cm, V = 1.15 ml. The extraction protocol included 5 ml of 7 M HNO_3 as a resin pre-condition step followed by matrix elution sequentially in 1 ml of 7 M HNO_3, 4 ml of 7 M HNO_3 and 2 ml of 0.05 M HNO_3. The elution of Sr was performed in 3 ml of 0.05 M HNO_3. After that, obtained solution was evaporated to dryness and admixed with 3% HNO_3 (v/v) for further isotope ratio measurement.

2.5. Sr isotope measurements

Isotope measurements were conducted in cleanrooms (class 10,000) of the Zavaritsky Institute of Geology and Geochemistry, Ekaterinburg, Russia. Sr isotope measurements were carried out using a MC ICP-MS Neptune Plus (Thermo Fisher Scientific, Germany) equipped by the ASX 110 FR sample introduction system (Teledyne CETAC, USA) fitted by PFA micro-flow nebulizer (50 μl min^{-1}) connected to a quartz spray chamber. Each individual acquisition consisted of 91 ratios collected at 8 s integrations with a 30 s baseline measurement before each block of 13 ratios. Blank correction was obtained on 3%(v/v) HNO_3 solution, using a configuration of 20 ratios of 8 s integration. The main parameters and cup configuration are provided in Table 2.

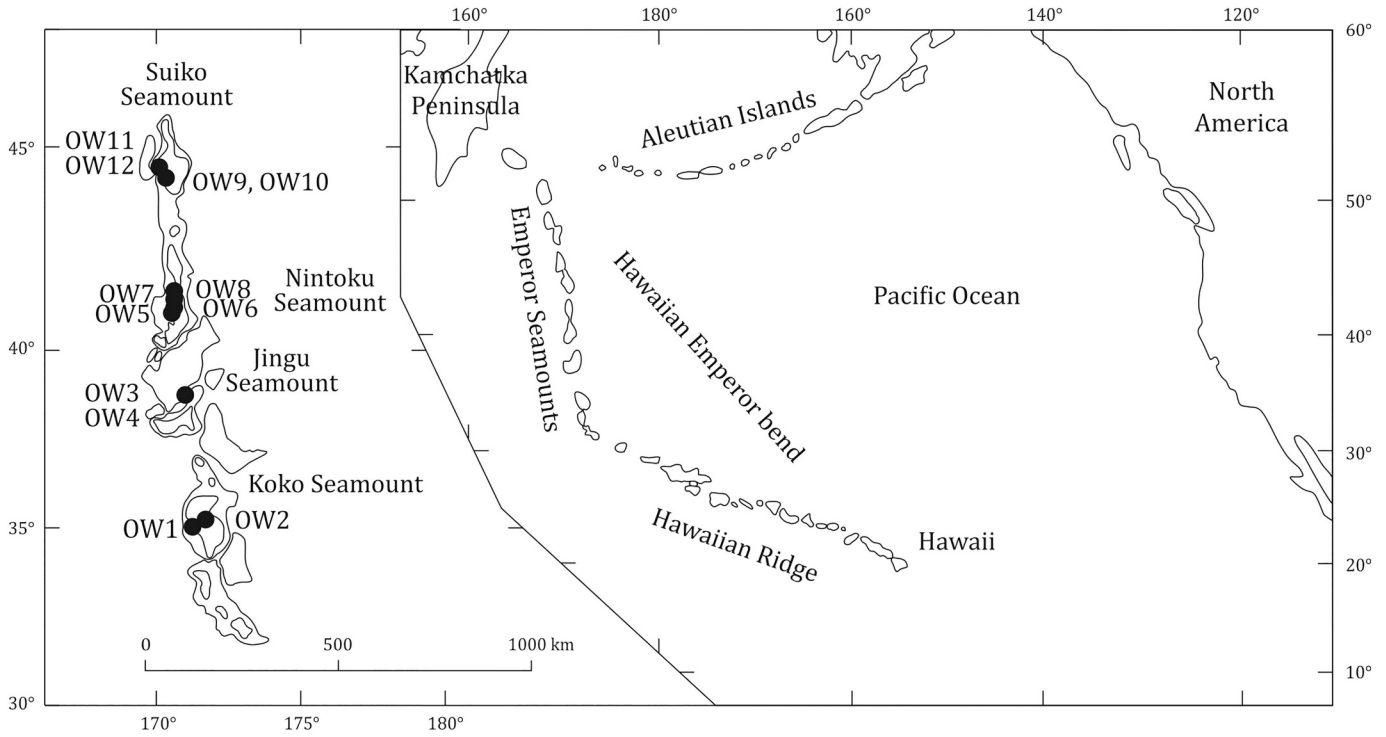

Fig. 1. Map of the studied area with the location and numbers of water samples (black circles).

In terms of mass-bias correction, the combination of exponential law normalization and bracketing technique was applied to measurement results. Thus, the $^{87}Sr/^{86}Sr$ ratio was normalized by the value of 88/86 = 8.37861. In addition, interference correction was provided by accounting of ^{86}Kr and ^{87}Rb by $^{83}Kr/^{86}Kr$ = 0.664162, $^{83}Kr/^{84}Kr$ = 0.201579 and $^{87}Rb/^{85}Rb$ = 0.386 ratios (also normalized). Subsequently, the normalized values were additionally corrected by the mean value variation of SRM-987 "bracketed" each two samples from the reference value of 0.710245 from the GeoReM database, http://georem.mpch-mainz.gwdg.de/.

In order to control the analytical procedure, SRM-987 Sr isotopic standard was measured on a regular basis yielding in $^{87}Sr/^{86}Sr$ = 0.710261 ± 20 (2SD, N = 257). The method precision was estimated as the within-laboratory standard uncertainty (2σ) obtained for SRM-987 and was 0.003%. The precision of each individual result (1 SE) during the sample measurement was within 25 ppm.

Table 2
Neptune Plus and ASX 110 FR instrumental parameters for Sr isotope measurement.

Instrumental parameters		Faraday Cup configuration	
Ar cooling	15 l min^{-1}	L4	82Kr
Ar auxiliary	1 l min^{-1}	L3	83Kr
Ar sample	1.08 l min^{-1}	L2	84Sr
Nebulizer flow	50 μl min^{-1}	L1	85Rb
Torch power	1200 W	C	86Sr
Wash time	60 s	H1	87Sr
Takeup time	50 s	H2	88Sr
Sensitivity for ^{88}Sr	20 V ppm^{-1}		

3. Results and discussion

The chemical composition of studied water samples is presented in Table 3. The cationic composition of deep and near-surface waters, in general, does not differ from each other. A considerable difference in the contents of Ti, Mn, Cu, Zr, Ag, Ta, Pb, Bi and Th is observed. The amount of these elements varies 10 times. Some regularities can be traced. The titanium and copper contents are an order of magnitude lower in samples taken in the area of Suiko seamount. The amount of silver is lower in the surface waters as compared to deep. Such behaviour of silver was noted earlier in the works of Yan Zhang et al. (Zhang

Table 1
Sampling coordinates and some parameters of water samples.

Sample	Depth, m	Seamount	Date	Coordinates	Water temperature, ° C	Salinity, ‰
OW1 2564	2564	Koko	13 Jul	N 35°01.972′; E 171°14.848′	1.69	34.64
OW2–10.5	10.5	Koko	13 Jul	N 35°14.547′; E 171°41.791′	22.99	34.69
OW3 2124	2124	Jingu	25 Jul	N 38°47.021′; E 171°05.297′	1.88	34.6
OW4–10	10	Jingu	27 Jul	N 38°43.152′; E 171°07.302′	18.99	34.56
OW5 1022 m	1022	Nintoku	06 Aug	N 40°55.737′; E 170°32.037′	3.11	34.36
OW6-10 m	10	Nintoku	06 Aug	N 41°04.873′; E 170°34.384′	17.92	34.12
OW7 1137 m	1117	Nintoku	07 Aug	N 41°17.842′; E 170°52.061′	2.84	34.41
OW8 2650 m	2650	Nintoku	07 Aug	N 41°31.270′; E 170°36.141′	1.65	34.64
OW9 1845 m	1845	Suiko	10 Aug	N 44°16.998′; E 170°22.611′	1.95	34.58
OW 10–10	10.2	Suiko	10 Aug	N 44°26.288′; E 170°20.974′	10.1	33.26
OW11 10.1	10.1	Suiko	11 Aug	N 44°42.109′; E 170°07.590′	11.92	32.87
OW12 1706 m	1706	Suiko	11 Aug	N 44°42.720′; E 170°06.644′	1.99	34.57

Table 3
Trace element (ppm) and REE (ppb) composition of the deep and near-surface waters of the southern part of the Emperor seamount chain.

Element	OW1 2564	OW2–10.5	OW3 2124	OW4–10	OW5 1022 m	OW6-10 m	OW7 1137 m	OW8 2650 m	OW9 1845 m	OW 10–10	OW11 10.1	OW12 1706 m
Li	0.09	0.12	0.11	0.11	0.09	0.12	0.11	0.13	0.1	0.11	0.1	0.13
B	0.46	0.6	0.5	0.5	0.46	0.6	0.5	0.7	0.5	0.6	0.5	0.7
Al	0.0022	0.0012	0.0009	0.002	0.0016	0.003	0.0016	0.0013	0.0021	0.0027	0.0013	0.019
Mn	0.0011	0.008	0.0009	0.0006	0.0005	0.0019	0.0007	0.0012	0.0007	0.0015	0.0005	0.0019
Ni	0.013	0.04	0.023	0.03	0.015	0.04	0.04	0.04	0.012	0.011	0.011	0.016
Cu	0.024	0.12	0.06	0.1	0.04	0.1	0.1	0.08	0.015	0.014	0.014	0.019
Zn	0.04	0.018	0.018	0.03	0.024	0.018	0.019	0.02	0.03	0.03	0.04	0.05
As	0.034	0.067	0.049	0.061	0.039	0.073	0.06	0.072	0.04	0.037	0.034	0.048
Se	0.129	0.21	0.17	0.18	0.134	0.23	0.19	0.25	0.107	0.102	0.117	0.099
Rb	0.18	0.26	0.23	0.23	0.19	0.27	0.24	0.3	0.15	0.14	0.16	0.16
Sr	15	17	17	16	15	19	16	22	14	12	14	15
Cs	0.00031	0.00033	0.00032	0.00033	0.00028	0.00031	0.0003	0.00032	0.00034	0.00034	0.00031	0.00039
Ba	0.019	0.0052	0.02	0.005	0.014	0.0057	0.015	0.022	0.02	0.009	0.008	0.024
Hg	< 0.00004	< 0.00004	< 0.00004	< 0.00004	< 0.00004	< 0.00004	< 0.00004	0.00004	0.000069	0.00019	0.000062	0.000118
Pb	0.00016	< 0.00001	< 0.00001	< 0.00001	< 0.00001	< 0.00001	< 0.00001	< 0.00001	0.0002	0.001	0.0001	0.0016
U	0.0021	0.0022	0.0022	0.0022	0.0019	0.0022	0.0021	0.0024	0.0025	0.0025	0.0021	0.0033
ppb												
La	0.013	0.023	0.014	0.017	0.009	0.025	0.025	0.070	0.011	0.015	0.008	0.022
Ce	0.010	0.001	0.003	0.007	0.007	0.003	0.005	0.042	0.006	0.009	0.006	0.017
Pr	0.007	0.022	0.012	0.015	0.008	0.022	0.021	0.019	0.007	0.007	0.006	0.008
Nd	0.014	0.023	0.015	0.030	0.011	0.024	0.030	0.036	0.012	0.014	0.013	0.017
Sm	0.008	0.005	0.006	0.006	0.006	0.007	0.010	0.009	0.009	0.014	0.009	0.007
Eu	0.002	0.001	0.002	0.002	0.001	0.001	0.001	0.001	0.001	0.003	0.002	0.002
Gd	0.007	0.003	0.010	0.008	0.009	0.005	0.004	0.004	0.004	0.008	0.006	0.008
Tb	0.002	0.002	0.002	0.002	0.002	0.004	0.003	0.012	0.003	0.004	0.002	0.004
Dy	0.008	0.012	0.009	0.007	0.007	0.009	0.010	0.007	0.006	0.006	0.005	0.010
Y	0.090	0.080	0.100	0.070	0.080	0.100	0.100	0.150	0.070	0.060	0.060	0.070
Ho	0.002	0.008	0.003	0.003	0.002	0.013	0.005	0.024	0.003	0.003	0.004	0.007
Er	0.004	0.009	0.006	0.004	0.005	0.008	0.004	0.010	0.007	0.005	0.003	0.009
Tm	0.001	0.001	0.001	0.001	0.001	0.001	0.001	0.001	0.001	0.002	0.001	0.001
Yb	0.006	0.002	0.007	0.004	0.004	0.002	0.004	0.004	0.005	0.004	0.004	0.005
Lu	0.001	< 0.0001	0.001	0.001	0.001	0.001	0.001	0.001	0.002	0.001	0.001	0.001
Sum REE	0.175	0.192	0.191	0.177	0.153	0.225	0.224	0.390	0.147	0.155	0.130	0.188
Ce/Ce*	0.221	0.008	0.044	0.082	0.155	0.024	0.042	0.261	0.139	0.190	0.170	0.286
LREE/HREE	0.366	1.328	0.488	0.809	0.389	1.006	1.079	0.981	0.254	0.304	0.350	0.391

Note: cerium anomaly was calculated as $Ce/Ce^* = Ce^{NASC}/(0.5La^{NASC} + 0.5Pr^{NASC})$, and LREE/HREE ratios as $LREE/HREE = (La^{NASC} + 2{\cdot}Pr^{NASC} + Nd^{NASC})/(Er^{NASC} + Tm^{NASC} + Yb^{NASC} + Lu^{NASC})$ using NASC-normalized La, Ce, Pr, Nd, Er, Tm, Yb and Lu contents.

et al., 2001). For the remaining elements, there is no clear correlation.

We compared the results with the IAPSO Standard Seawater, SSW (Summerhayes and Thorpe, 1996), prepared from natural open-ocean water collected from the surface waters of the mid-Atlantic. The distribution pattern of elements in deep and near-surface waters is similar to each other (with the exception of the points indicated above). When compared to standard water, the studied samples are enriched in Mn, Ni, Cu, Zn, As, Se, Hg, and Pb on average by two orders of magnitude, Al on average by 4–6 times (Fig. 2). This difference can be explained by the fact that the river and atmospheric flow of matter into the waters of the North Atlantic is higher than in the northern part of the Pacific Ocean (Bruland and Franks, 1983), and the chemical composition of the incoming flows is also different. Another reason is the difference in currents, especially in those providing deep waters enriched/depleted in certain elements (Chester, 1990).

Several types of trace element distribution with depth are known in the literature (Chester, 1990; Bruland and Lohan, 2006), depending on how they participate in the biological cycle. For example, Zn concentration profile in water is similar to the Si profile. The maximum concentration of these elements is achieved at a depth, where zinc content may be an order of magnitude greater than on the surface (Bruland et al., 1978; Chester, 1990). Such regularity is not observed for the studied water samples. Zn concentrations both in surface and bottom waters remain the same. We did not filter water and studied suspended, dissolved material and the organic component together. Possibly, a constant Zn concentration in water can be explained by the

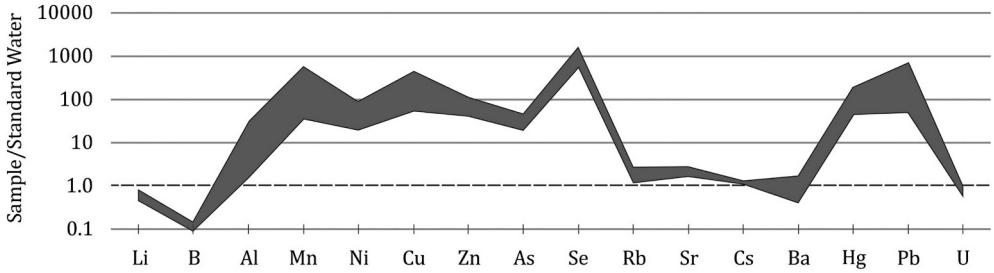

Fig. 2. Comparison of the chemical composition (Summerhayes and Thorpe, 1996) of the IAPSO standard sea water (dashed line) and the studied samples (gray field).

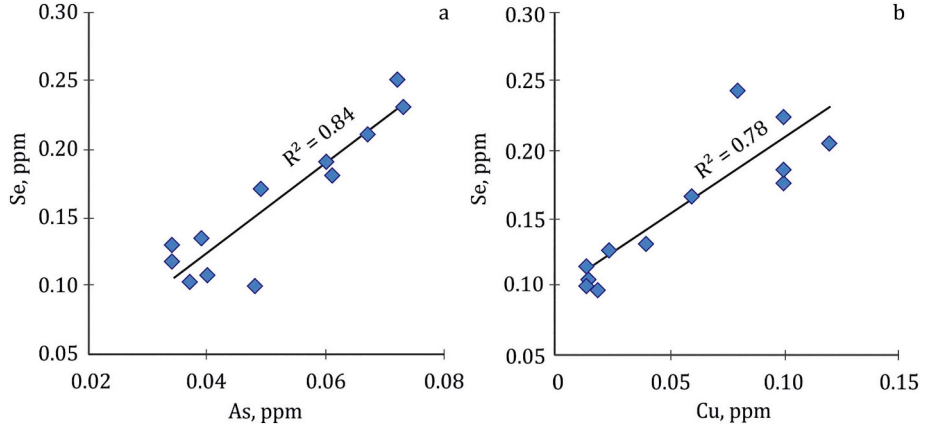

Fig. 3. The relationship between the content of Se and As (a), Se and Cu (b).

balance between the matter that gets into the biological cycle and the one that is released from it. That is, plankton is not inclined to accumulate and concentrate Zn, therefore its concentration remains constant.

A detailed examination of the trace element behaviour of the studied samples has revealed a direct correlation in Se—Cu and Se—As pairs over the entire water column (Fig. 3). Se and Cu are of great biological importance, while As, not being an essential element in biochemical processes, is also very actively accumulated by living organisms (Ivanov, 1996). According to the work by Galina Leonova et al. (Leonova et al., 2013), these elements reside in seawater in labile (bioavailable) forms and are accumulated by zooplankton to a great extent. The enrichment coefficients for Se, Cu, and As relative to bottom sediments are rather high – about 100 (Leonova et al., 2013). Thus, the correlations within Se—Cu and Se—As pairs can indicate a significant plankton contribution into the concentrations of these elements in the collected water samples. The concentration changes in surface (warm waters) confirm the hypothesis about the microorganism influence on the water composition. A noticeable increase in Cu, As, and Se content with an increase in the temperature of the surface layer was observed. This fact can be interpreted as an increase in the biological productivity of water with increasing layer temperature.

The distribution of shale-normalized rare-earth elements (normalized to the North American shale - NASC (Haskin et al., 1968)) indicates a weak enrichment with heavy REE as compared to light REE and a negative cerium anomaly (Fig. 5). The magnitude of this anomaly (Ce/Ce*) varies from very significant (0.08) to small (0.28). The cerium anomaly grows with increasing temperature of the surface layer (Fig. 4), that is, the amount of cerium relative to neighboring REE decreases. A negative cerium anomaly is formed under the surface conditions due to the cerium oxidation (Sholkovitz et al., 1993). Moreover, the arising cerium deficiency among dissolved REE is compensated by the presence of a positive anomaly in suspended REE (Masuzawa and Koyama, 1989; Bertram and Elderfield, 1993; Sholkovitz et al., 1993; Lerche and Nozaki, 1998; Tachikawa et al., 1999). A negative correlation (Cc = −0.98) of cerium anomaly with Se content (an important nutrient element and an indicator of bioproductivity) may indicate the possible role of biota in Ce oxidation (Fig. 6).

The isotopic composition of Sr varies from 0.70891 to 0.70917 with an average of 0.70910 ± 0.00007 (Table 4, Fig. 7). $^{87}Sr/^{86}Sr$ ratio in deep waters is less variable and corresponds to the average value for the world ocean (0.70913 ± 0.00004). The isotopic composition of Sr in surface waters is less radiogenic (0.70906 ± 0.00010). Fig. 8a shows the dependence of Sr isotopic composition and water salinity. From this graph it can be noted that isotopic ratios correlate with salinity ($Cc_{Warm\ Water}$ = −0.74) and are inherent only in surface warm waters (t ° 10–23 °C). The same situation is observed between the Sr content and salinity ($Cc_{Warm\ Water}$ = 0.70, Fig. 8b). In this case, there is no

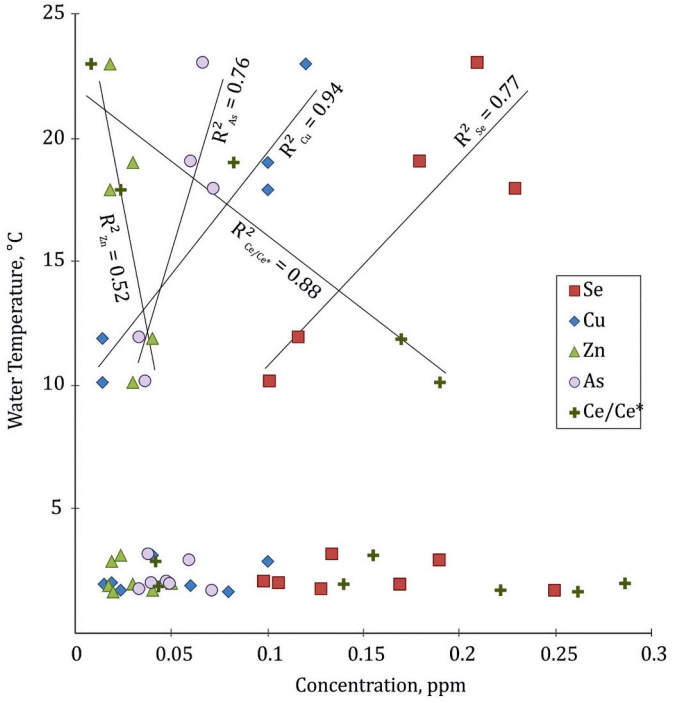

Fig. 4. Change in the concentration of Se, Cu, Zn, As and cerium anomaly with temperature. R^2 is coefficient of correlation between the temperature of surface waters and the content of elements in them. The graph shows that Zn, being a biogenic element, behaves latently (R^2 is about 0.5) and its content does not change with temperature.

dependence between Sr isotopic composition and its concentration ($Cc_{Warm\ Water}$ = − 0.45, Fig. 8c).

Strontium in seawater is very mobile, its residence time is 5 million years (Taylor and McLennan, 1985), and the mixing time of ocean waters is only about one thousand years (Broecker and Peng, 1982; Elderfield and Greaves, 1982). Therefore, on a geological time scale, the isotopic composition of ocean water is constant at every point.

Nevertheless, the distribution of Sr isotope ratios in coastal waters was found to be rather complicated with a nonhomogeneous vertical pattern (variation up to 70 ppm) across the different water sections of the Pacific coast (Huang et al., 2011). Surface enrichment in ^{87}Sr was attributed to the input of long-range transport of Eolian dust from eastern Asia (Huang et al., 2011). Seawater Sr isotopic composition changed in the upper 200 m of the Southern Okinawa Trough and was highly correlated with salinity, indicating a mixing between more and less radiogenic components. The significant $^{87}Sr/^{86}Sr$ variations of

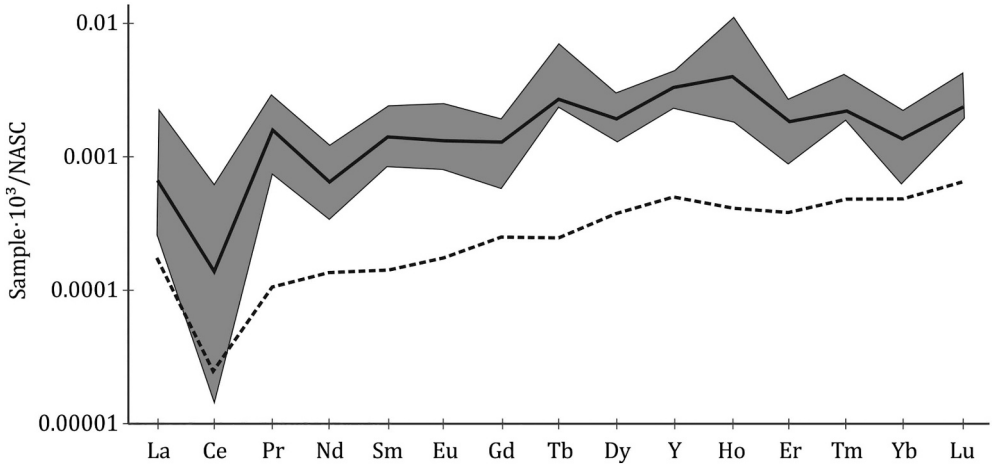

Fig. 5. NASC-normalized REE composition of near-surface and deep waters - gray field, thick line — average content for all samples. The graph also shows the REE distribution in IAPSO Standard Seawater (dashed line). The graph indicates that the Atlantic water is depleted in REE as compared with the Pacific.

seawater across vertical profiles along the Kao-ping Canyon suggested dynamic mixing affected by continental inputs (i.e., river runoff and submarine groundwater discharge) in the studied region (Huang et al., 2011). Moreover, the enhanced submarine groundwater discharge fluxes could be attributed to rapid responses of shallow and deep aquifers to the heavy rainfall event (Oliveira et al., 2006).

In our study, the independent two-sample *t*-test was used to confirm that the near-surface water layer was significantly different from the deeper one by Sr isotopic ratios ($p < .05$).

During staying and sampling in the area of the Koko, Jingu and Nintoku seamounts (southward of 44° N), it rained briefly daily (up to 20 mm per day according to the https: //earth.nullschool.net/ website). It is apparently the influence of meteoric water that can explain the decrease in the $^{87}Sr/^{86}Sr$ ratio in the near-surface layer. The Sr isotopic composition of atmospheric precipitation in Japan (areas of the cities of Sapporo 0.70852, Morioka 0.70844 and Kumamoto 0.70885, Kawakami forest 0.70766 (Nakano and Tanaka, 1997; Nakano et al., 2006)) is found to be lower than sea water. We took the rainwater isotopic composition from the articles of Takanori Nakano et al. (Nakano et al., 2006; Nakano and Tanaka, 1997) for one end-member of the mixing Eq. (1), and the $^{87}Sr/^{86}Sr$ ratio of deep seawater for the second. According to the mixing equation, the proportion of meteoric water in the layer at a depth of 10 m is 0.010%.

$$f = \frac{(A_2)\bullet(x_m - x_2)}{[A_1]\bullet(x_1 - x_m) + (A_2)\bullet(x_m - x_2)} \quad (1)$$

where (A) is the Sr concentration in rain and ocean water indicated by the indices 1 and 2, respectively; *x* is $^{87}Sr/^{86}Sr$ ratio at the same end-points, x_m - isotopic composition of surface water (0.70906).

In our opinion, even a small fraction of rain water was able to significantly (higher than the measurement error) bias Sr isotopic ratio in the near-surface water due to its dilution by low-Sr fresh water (more than ten-fold lower than in ocean water (Nakano and Tanaka, 1997)) with low $^{87}Sr/^{86}Sr$ ratio, taking into account the permanent character of atmospheric precipitation and its high daily amount. Moreover, the fraction of rain water at a depth of less than 10 m could be higher, reaching its maximum values in the uppermost layers of sea water. Unfortunately, a more stratified sample collection of the surface waters couldn't be realized, and thus a more detailed elaboration of near-surface water layer has stayed beyond the scope of our present work.

The Suiko seamount is located northward of 44° N, at a distance of almost 300 km from the Nintoku seamount. Water samples in that area

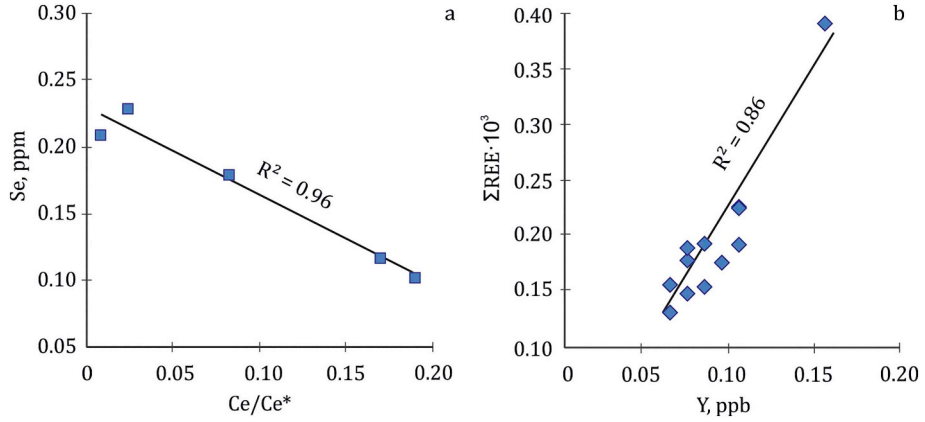

Fig. 6. (a) Inverse relationship between Se and cerium anomaly in surface waters. (b) A direct correlation between the sum of REE and Y indicates their similar behaviour in ocean water.

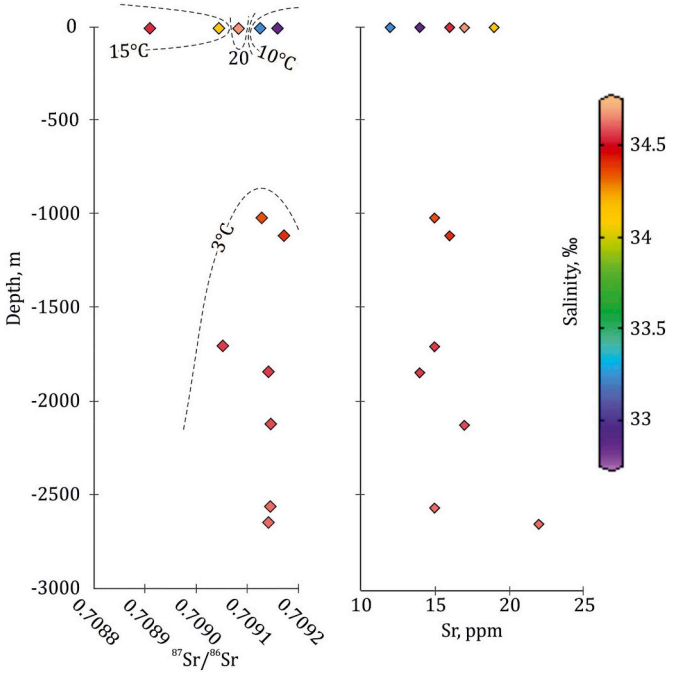

Fig. 7. Sr isotopic composition (a) and content (b) in water samples distributed over depth. Colour of diamonds depend on their salinity, dashed lines are temperature of water, °C.

were taken in clear, calm weather. Precipitation was absent in the area for ten days. According to the https://earth.nullschool.net/ website the rain front was in that region until 07/31/2019, then moved eastward. Probably, this time was enough for the near-surface diluted water layer to mix with deep waters. This apparently caused the homogeneity of the Sr isotopic composition both at depth and in the near-surface layer. The exception was the last sample from a depth of 1706 m with $^{87}Sr/^{86}Sr$ ratio of 0.70905.

A change in the composition of surface waters can also be traced in the behaviour of the cerium anomaly. The water diluted by rain has the largest Ce anomaly (Ce/Ce* 0.008–0.02). The difference between Ce/Ce* in deep and near-surface waters can reach one order of magnitude (Table 3). The Ce/Ce* value of the waters above Suiko seamount is 0.17–0.19 and almost does not differ from deep water.

Table 4
Sr content and isotopic composition of near-surface and bottom water of the southern part of the Emperor seamount chain.

Sample	Depth, m	Seamount	Sr, mg/l	$^{87}Sr/^{86}Sr$	2SE, abs
OW1 2564	2564	Koko	15	0.709145	0.000011
OW2–10.5	10.5	Koko	17	0.709083	0.000085
OW3 2124	2124	Jingu	17	0.709146	0.000011
OW4–10	10	Jingu	16	0.708910	0.000020
OW5 1022 m	1022	Nintoku	15	0.709128	0.000007
OW6-10 m	10	Nintoku	19	0.709045	0.000016
OW7 1137 m	1117	Nintoku	16	0.709172	0.000009
OW8 2650 m	2650	Nintoku	22	0.709141	0.000015
OW9 1845 m	1845	Suiko	14	0.709141	0.000010
OW 10–10	10.2	Suiko	12	0.709125	0.000008
OW11 10.1	10.1	Suiko	14	0.709159	0.000008
OW12 1706 m	1706	Suiko	15	0.709052	0.000011

4. Conclusions

Seawater Sr isotopic ratios are a sensitive and powerful tool for tracing the dynamic mixing processes of water masses and their migration pathway. Despite Sr isotopic composition of the ocean is considered to be constant at any point any time, there are local zones with varying $^{87}Sr/^{86}Sr$ ratio. One of the reasons for this can be the influence of meteoric (rain) waters. Moreover, the penetration of rainwater and dilution is very significant: it is quite pronounced at a depth of 10 m from the surface, both at the chemical and Sr isotopic levels. It is likely that the vertical movement of the matter plays an important role in this process, as many works point out (for example (Nozaki and Alibo, 2003)), and such mixing occurs rather quickly in a matter of days. High vertical mixing rates are responsible for balancing the Sr isotopic composition in the area of the Suiko seamount.

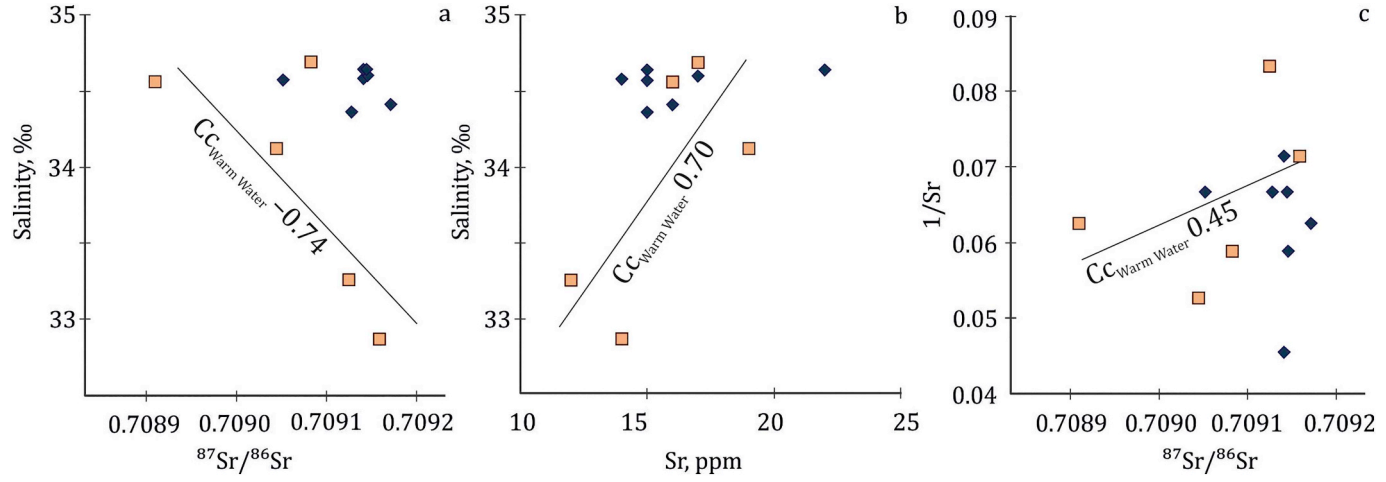

Fig. 8. (a) The regular decrease in the $^{87}Sr/^{86}Sr$ ratio in near-surface waters (squares) with a decrease in salinity is shown. No dependence is observed for deep waters (diamonds). (b) A direct relationship between salinity and Sr concentration of near-surface waters (squares) and the absence of inter-relationship in deep waters (diamonds). (c) A graph showing the absence of a relationship between the Sr content (here 1/Sr) and its isotopic composition. $Cc_{Warm\ Water}$ - correlation coefficient for surface warm water.

Acknowledgments

The authors are grateful to the Head of 86th voyage of the R/V "Akademik M.A. Lavrentiev" Tatyana Nikolaevna Dautova for organizing the work, Oleg Gennadievich Borzykh, Nikita Sergeevich Polonik, Alexei Alexandrovich Legkodimov, Alexei Mikhailovich Koltunov and Alexei Mikhailovich Asavin for their help with water sampling.

We thank the Reviewers for the important comments and constructive suggestions, which helped us to improve the quality of the manuscript greatly.

Participation in the 86th voyage of the R/V "Akademik M.A. Lavrentiev" was possible due to a grant from the Russian Foundation for Basic Research № 18-05-00436. Chemical and isotopic investigations were carried out as a part of the state assignments of the GEOCHI RAS (state assignment No. 0137-2019-0015) and the IGG UB RAS (state registration number AAAA-A18-118053090045-8).

References

de Villiers, S., 1999. Seawater strontium and Sr/Ca variability in the Atlantic and Pacific Oceans. Earth Planet. Sci. Lett. 171, 623–634.

GeoReM database http://georem.mpch-mainz.gwdg.de/ (accessed 06 January 2020).

Bach, W., Humphris, S.E., 1999. Relationship between the Sr and O isotope compositions of hydrothermal fluids and the spreading and magma-supply rates at oceanic spreading centers. Geology 27, 1067–1070.

Banner, J.L., 2004. Radiogenic isotopes: systematics and applications to earth surface processes and chemical stratigraphy. Earth Sci. Rev. 65, 141–194.

Bertram, C.J., Elderfield, H., 1993. The geochemical balance of rare earth elements and neodymium isotopes in the oceans. Geochim. et Cosmochim. Acta. 57, 1957–1986.

Broecker, W.S., Peng, T.H., 1982. Tracers in the Sea. Lamont-Doherty Geol. Obs, Palisades, New York.

Bruland, K.W., Franks, R.P., 1983. Mn, Ni, Zn and Cd in the western North Atlantic. In: Trace Metals in Sea Water. Plenum, New York, pp. 395–414.

Bruland, K.W., Lohan, M.C., 2006. Controls of trace metals in seawater. The oceans and marine geochemistry. 6, 23–47.

Bruland, K.W., Knauer, G., Martin, J., 1978. Zinc in Northeast Pacific waters. Nature. 271, 741–743.

Burke, W.H., Denison, R.E., Hetherington, E.A., Koepnick, R.B., Nelson, H.F., Otto, J.B., 1982. Variation of seawater $^{87}Sr/^{86}Sr$ throughout Phanerozoic time. Geology. 10 (10), 516–519.

Chester, R., 1990. Trace Elements in the Oceans. Marine Geochemistry. Unwin Hyman, London.

Clague, D.A., Dalrymple, G.B., 1987. The Hawaiian-emperor volcanic chain. Part I. geologic evolution. Volcanism in Hawaii. 1, 5–54.

Dalrymple, G.B., Clague, D.A., 1976. Age of the Hawaiian-emperor bend. Earth Planet. Sci. Lett. 31, 313–329.

Darnitsky, V.B., 2010. Oceanological Processes near Seamounts and Ridges of the Open Ocean. TINRO Center, Vladivostok (in Russian).

Davis, A.C., Bickle, M.J., Teagle, D.A.H., 2003. Imbalance in the oceanic strontium budget. Earth Planet. Sci. Lett. 211, 173–187.

DePaolo, D.J., 1987. Correlating rocks with strontium isotopes. Geotimes. 32 (12), 16–18.

Elderfield, H., Gieskes, J.M., 1982. Sr isotopes in interstitial waters of marine sediments from Deep Sea drilling project cores. Nature. 300, 493–497.

Elderfield, H., Greaves, M.J., 1982. The rare earth elements in seawater. Nature. 296, 214–219.

England, M.H., Maier-Reimer, E., 2001. Using chemical tracers to assess ocean models. Rev. Geophys. 39 (1), 29–70.

Faure, G., 1986. Principles of Isotope Geology, 2nd ed. Willey et Sons, New York.

Gregg, M.C., 1991. The study of mixing in the ocean: a brief history. Oceanography. 4 (1), 39–45.

Halverson, G.P., Dudás, F.Ö., Maloof, A.C., Bowring, S.A., 2007. Evolution of the $^{87}Sr/^{87}Sr$ composition of Neoproterozoic seawater. Paleogeogr. Paleoclimatol. Paleoecol. 256 (3–4), 103–129.

Halverson, G.P., Wade, B.P., Hurtgen, M.T., Barovich, K.M., 2010. Neoproterozoic chemostratigraphy. Precambrian Res. 182 (4), 337–350.

Haskin, L.A., Haskin, M.A., Frey, F.A., Wildeman, T.R., 1968. Relative and absolute terrestrial abundances of the rare earths. In: Origin and Distribution of the Elements. Pergamon, pp. 889–912.

Hodell, D.A., Mueller, P.A., McKenzie, J.A., Mead, G.A., 1989. Strontium isotope stratigraphy and geochemistry of the late Neogene ocean. Earth Planet. Sci. Letters. 92 (2), 165–178.

Huang, K.-F., You, C.-F., Chung, C.-H., Lin, I.-T., 2011. Nonhomogeneous seawater Sr isotopic composition in the coastal oceans: a novel tool for tracing water masses and submarine groundwater discharge. Geochem. Geophys. Geosyst. 12, Q05002. https://doi.org/10.1029/2010GC003372.

Ivanov, V.V., 1996. V. 3: Rare p-elements. In: Burenkova, E.K. (Ed.), Ecological Geochemistry of Elements: Handbook. Nedra, Moscow, pp. 1996 (352 p. in Russian).

Jenkins, W.J., 2004. Tracers of Ocean Mixing. The Oceans and Marine Geochemistry. Elsevier, London.

Kasyanova, A.V., Streletskaya, M.V., Chervyakovskaya, M.V., Kiseleva, D.V., 2019. A method for $^{87}Sr/^{86}Sr$ isotope ratio determination in biogenic apatite by MC-ICP-MS using the SSB technique. AIP Conference Proceedings. 2174, 020028.

Keller, R.A., Fisk, M.R., White, W.M., 2000. Isotopic evidence for Late Cretaceous plume–ridge interaction at the Hawaiian hotspot. Nature 405 (6787), 673–676. https://doi.org/10.1038/35015057.

Kuznetsov, A.B., Gorokhov, I.M., Semikhatov, M.A., 2014. The Sr isotope chemostratigraphy as a tool for solving stratigraphic problems of the Upper Proterozoic (Riphean and Vendian). Stratigr. Geol. Correl. 22 (6), 553–575.

Kuznetsov, A.B., Gorokhov, I.M., Semikhatov, M.A., 2018. Strontium isotope stratigraphy: principles and state of the art. Stratigr. Geol. Correl. 26 (4), 367–386.

Leonova, G.A., Bobrov, V.A., Bogush, A.A., Bychinskii, V.A., 2013. Concentration of chemical elements by zooplankton of the White Sea. Oceanology. 53, 54–70.

Lerche, D., Nozaki, Y., 1998. Rare earth elements of sinking particulate matter in the Japan Trench. Earth Planet. Sci. Lett. 159, 71–86.

Masuzawa, T., Koyama, M., 1989. Settling particles with positive Ce anomalies from the Japan Sea. Geophys. Res. Lett. 16 (6), 503–506.

McArthur, M., Howaith, R.J., Bailey, T.R., 2001. Strontium isotope stratigraphy: LOWESS version 3: best fit to the marine Sr-isotope curve for 0-509 ma and accompanying look-up table for deriving numerical age. J. Geol. 109, 155–170.

McArthur, J.M., Howarth, R.J., Shields, G.A., 2012. Strontium isotope stratigraphy. The geologic time scale. 1, 127–144.

Muynck, D.D., Huelga-Suarez, G., Heghe, L.V., Degryse, P., Vanhaecke, F., 2009. Systematic evaluation of a strontium-specific extraction chromatographic resin for obtaining a purified Sr fraction with quantitative recovery from complex and Ca-rich matrices. J. Anal. At. Spectrom. 24, 1498–1510.

Nakano, T., Tanaka, T., 1997. Strontium isotope constraints on the seasonal variation of the provenance of base cations in rain water at Kawakami, central Japan. Atmos. Environ. 31, 4237–4245.

Nakano, T., Morohashi, S., Yasuda, H., Sakai, M., Aizawa, Sh., Shichi, K., Morisawa, T., Takahashi, M., Sanada, M., Matsuura, Y., Sakai, H., Akama, A., Okada, N., 2006. Determination of seasonal and regional variation in the provenance of dissolved cations in rain in Japan based on Sr and Pb isotopes. Atmos. Environ. 40 (38), 7409–7420.

Nozaki, Y., Alibo, D.S., 2003. Importance of vertical geochemical processes in controlling the oceanic profiles of dissolved rare earth elements in the northeastern Indian Ocean. Earth Planet. Sci. Lett. 205 (3–4), 155–172.

Oliveira, J., Costa, P., Braga, E.S., 2006. Seasonal variation of ^{222}Rn and SGD fluxes to Ubatuba embayments, São Paulo. J. Radioanal. Nucl. Chem. 269, 689–695. https://doi.org/10.1007/s10967-006-0287-2.

Sawaki, Y., Ohno, T., Tahata, M., Komiya, T., Hirata, T., Maruyama, S., Windley, B.F., Han, J., Shu, D., Li, Y., 2010. The Ediacaran radiogenic Sr isotope excursion in the Doushantuo Formation in the Three Gorges area, South China. Precambrian Res. 176 (1–4), 46–64.

Sholkovitz, E.R., Church, T.M., Arimoto, R., 1993. Rare earth element composition of pricipitation, pricipitation particles, and aerosols. Journal Geophys. Research. 98 (11), 20587–20599.

Stewart, R.H., 2008. Introduction to Physical Oceanography. Texas A&M University, College Station.

Summerhayes, C.P., Thorpe, S.A., 1996. Oceanography – An Illustrated Guide. Manson Publishing, London.

Tachikawa, K., Jeandel, C., Vangriesheim, A., Dupre, B., 1999. Distribution of rare earth elements and neodymium isotopes in suspended particles of the tropical Atlantic Ocean (EUMELI site). Deep Sea Research, Part I. 46, 733–755.

Taylor, S.R., McLennan, S.M., 1985. The Continental Crust: Its Composition and Evolution. Blackwell, Oxford.

Zhang, Y., Amakawa, H., Nozaki, Y., 2001. Oceanic profiles of dissolved silver; precise measurements in the basins of western North Pacific, Sea of Okhotsk, and the Japan Sea. Mar. Chem. 75, 151–162.